Theoretical and experimental determination of the crystal structures of cesium-molybdenum chloride

Norio Saito, Yoshiki Wada, Pierric Lemoine, Stéphane Cordier, Fabien Grasset, Takeo Ohsawa, Noriko Saito, Jeffrey S. Cross, Naoki Ohashi

Theoretical and experimental determination of the crystal structures of cesium-molybdenum chloride

Norio Saito[1,2,3], Yoshiki Wada[2,3], Pierric Lemoine[4], Stéphane Cordier[4], Fabien Grasset[2,3,5], Takeo Ohsawa[2,3], Noriko Saito[3], Jeffrey S. Cross[1], Naoki Ohashi[2,3,6]*

[1]*Department of Metallurgy and Ceramics Science, Tokyo Institute of Technology, Meguro, Tokyo 152-8551, Japan*

[2]*Optical and Electronic Materials Unit, National Institute for Materials Science (NIMS), Tsukuba, Ibaraki 305-0044, Japan*

[3]*NIMS-Saint-Gobain Center of Excellence for Advanced Materials, NIMS, Tsukuba, Ibaraki 305-0044, Japan*

[4]*Institut des Sciences Chimiques de Rennes (ISCR; UMR 6226), University of Rennes 1 (UR1), General Leclerc, Rennes 35042, France*

[5]*Laboratory for Innovative Key Materials and Structures (LINK; UMI 3629), NIMS, Tsukuba, Ibaraki 305-0044, Japan*

[6]*Materials Research Center for Element Strategy (MCES), Tokyo Institute of Technology, Yokohama 226-8503, Japan*

E-mail: OHASHI.Naoki@nims.go.jp

We herein report the structure-property relationships of the octahedral molybdenum metal cluster compound, $Cs_2[Mo_6Cl_{14}]$. Using purified samples, we attempted to determine if $Cs_2[Mo_6Cl_{14}]$ possesses crystalline polarity. Heat treatment was performed prior to characterization to remove impurities, as X-ray powder diffraction and Fourier transformation infrared spectroscopy studies suggested the unit cell of $Cs_2[Mo_6Cl_{14}]$ expanded with the insertion of water molecules and/or hydroxyl moieties. Geometry optimization and total energy calculations by density functional theory calculations were conducted to determine whether $Cs_2[Mo_6Cl_{14}]$ crystallizes in centrosymmetric ($P\bar{3}1c$) or non-centrosymmetric ($P31c$) space groups. Furthermore, the results of the optical studies, along with the absence of a second harmonic generation, and the observation of a strong third harmonic generation, supported the hypothesis that inversion symmetry exists in the $Cs_2[Mo_6Cl_{14}]$ lattice. The space group of $Cs_2[Mo_6Cl_{14}]$ was therefore identified as $P\bar{3}1c$ symmetry.

1. Introduction

Molybdenum(II) halide cluster complexes, $[Mo_6X^i_8X^a_6]^{2-}$ (X = halogen, i = inner, and a = apical),[1] consist of an octahedral Mo_6 cluster bonded to 14 X ligands. Eight X^i ligands are coordinated to the Mo_6-cluster on the inner face capping positions, while the remaining six X^a ligands lie in terminal apical positions. A range of $[Mo_6X^i_8X^a_6]^{2-}$ complexes exhibiting different chemical properties can be synthesized by substituting X^i and X^a with different halogen ions.[2-4] As the formal charge of the $[Mo_6X^i_8X^a_6]^{2-}$ complexes is $-2e$, this species can be crystallized with counter cations to give $A_m[Mo_6X^i_8X^a_6]$ compounds (A = counter cation, m = 2 for monovalent, and m = 1 for divalent).[5] Owing to their large size, $[Mo_6X^i_8X^a_6]^{2-}$ complexes can be crystallized not only with elemental inorganic cations (e.g., Cs^+) but also with organic molecular cations. For example, Saito et al.[6] explored the formation of a number of $A_m[Mo_6X^i_8X^a_6]$ crystals employing various functional organic molecules as the A-cation. In addition, the incorporation of anionic $[Mo_6X^i_8X^a_6]^{2-}$ cluster units in organic polymer matrices has been widely developed to produce nanocomposites combining the photophysical properties of clusters with the mechanical and optical properties of polymers.[7]

A number of studies have reported the superconductivity of the so-called Chevrel compounds, i.e., metal chalcogenide cluster complexes with the formula $Mo_6Q^i_2Q^{i\text{-}a}{}_{6/2}Q^{a\text{-}i}{}_{6/2}$ (Q = chalcogen),[8] and as such, investigations focusing on the electric transport properties of Chevrel compounds, such as $Pb[Mo_6S_8]$, have been conducted.[9] In contrast, compounds based on $[Mo_6X^i_8X^a_6]^{2-}$ complexes, characterized by their wide energy band gaps, have recently been studied from the viewpoint of optoelectronic applications, such as phosphors,[10-12] photocatalysts,[13-15] and optical oxygen sensors.[16] In particular, $[Mo_6X^i_8X^a_6]^{2-}$ complexes, exhibiting broadband red luminescence under UV or blue light,[10] have received increasing attention, since phosphors with efficient broadband visible emission under blue light excitation are important for the improvement of solid-state lighting efficiency.[17,18] Hence, we were interested in studying the electronic structures of $[Mo_6X^i_8X^a_6]^{2-}$ complexes and $[Mo_6X^i_8X^a_6]^{2-}$-based compounds. Indeed, we recently reported the presence of additional overlapping emission at low temperatures, and the emission process for $[Mo_6Br_{14}]^{2-}$-based complexes.[19]

A particularly interesting feature of the luminescence properties of $[Mo_6X^i_8X^a_6]^{2-}$-based compounds is a large Stokes shift.[10] Such optical properties depend on the combination of X^i and X^a,[20,21] and so the effects of halogen substitution on the electronic structure of these

compounds and their excited states were investigated.[22,23] Based on these investigations into the electronic structure of the $[Mo_6X^i_8X^a_6]^{2-}$ complexes, theoretical simulations have been adopted. However, the majority of studies have utilized molecular simulation techniques where the $[Mo_6X^i_8X^a_6]^{2-}$ complexes were regarded as isolated charged molecules. For example, cluster model calculations on $[Mo_6X^i_8X^a_6]^{2-}$,[23,24] $[W_6X^i_8X^a_6]^{2-}$,[25] and $[Re_6Q^i_8X^a_6]^{4-}$ (Q^i = S or Se)[26,27] have been reported. However, these studies utilized molecular orbital calculations for ionized complexes. It is therefore evident that further theoretical investigations into the crystalline form of $[Mo_6X^i_8X^a_6]^{2-}$-based compounds are required to reach a deeper understanding of such compounds, in particular in relation to their crystalline and electronic structures.

We herein chose to focus on $Cs_2[Mo_6Cl_{14}]$, which is a representative $[Mo_6X^i_8X^a_6]^{2-}$-based compound with a relatively simple chemical composition. Two previous reports have been published focusing on the crystal structure of the trigonal $Cs_2[Mo_6Cl_{14}]$. One study reported the lattice parameters to be a_0 = 0.977 nm and c_0 = 1.422 nm,[5] while the other quoted a_0 = 0.983(5) nm and c_0 = 1.431(3) nm.[28] These values differ significantly, and even if the $P31c$ space group was suggested,[28] the lattice symmetry of the trigonal $Cs_2[Mo_6Cl_{14}]$ was not successfully confirmed.[5,28] Although it appears that the symmetry of both $Cs_2[Mo_6Br_{14}]$ and $Cs_2[Mo_6I_{14}]$ belongs to the $P\bar{3}1c$-group,[29] it is not clear whether the trigonal $Cs_2[Mo_6Cl_{14}]$ possesses $P\bar{3}1c$ or $P31c$ symmetry (see Fig. 1). We therefore focused on determination of the crystalline and electronic structures of trigonal $Cs_2[Mo_6Cl_{14}]$ by density functional theory (DFT) calculations. In particular, plane wave-based DFT simulation codes for the periodic lattice system were used to study the electronic structure of trigonal $Cs_2[Mo_6Cl_{14}]$. In addition to theoretical simulations, we experimentally examined the crystal structure of trigonal $Cs_2[Mo_6Cl_{14}]$ using both X-ray powder diffraction (XRD) and neutron powder diffraction (NPD). Interestingly, we showed that molecules in an experimental environment (e.g., in water) could be inserted into the unoccupied trigonal site of the $Cs_2[Mo_6Cl_{14}]$ lattice without altering the trigonal lattice. In addition, using powder diffraction results, geometry optimization from DFT calculations, and optical studies employing an fs-pulsed laser for second harmonic generation (SHG), we propose an explanation into the crystal structure ambiguity of the trigonal $Cs_2[Mo_6Cl_{14}]$. We herein report our experimental and theoretical investigations into the crystal structure of $Cs_2[Mo_6Cl_{14}]$.

2. Materials and methods

2.1 Sample preparation

The synthesis of $Cs_2[Mo_6Cl_{14}]$ was performed according to a method derived from that reported by Healy et al.[28] Initially, $(H_3O)_2[Mo_6Cl_{14}]\cdot 7H_2O$ was prepared as single crystals using a method reported by Koknat et al.[30] Subsequently, $(H_3O)_2[Mo_6Cl_{14}]\cdot 7H_2O$ (10 g, 8.20 mmol) and CsCl (2.75 g, 16.4 mmol) were dissolved separately in ethanol (10 mL) and the resulting solutions were heated to reflux. The CsCl solution was then added to the cluster solution under stirring. Following evaporation of the solvent to dryness, $Cs_2[Mo_6Cl_{14}]$ was extracted from the remaining solid by dissolution in acetone and further evaporation using a Rotavapor R-100 (Buchi Labortechnik). Finally, the $Cs_2[Mo_6Cl_{14}]$ powder was crystallized from the filtrate by solvent evaporation. The resulting powder was stored under air at room temperature.

2.2 Characterization and analyses

Structural characterization was performed by XRD using a RINT-Ultima III diffractometer (Rigaku) with monochromatic CuKα radiation (λ = 0.15418 nm). Lattice constants were refined using the least-squares method by sampling >10 observed XRD peaks.

Prior to carrying out XRD measurements, the samples were heated under different atmospheres to examine if water intercalation in $Cs_2[Mo_6Cl_{14}]$ caused degradation in crystallinity. The $Cs_2[Mo_6Cl_{14}]$ powder was heated at 150–200°C for 60–180 min under air, or in pure N_2 gas with O_2 and H_2O concentrations of <0.1 ppm. To confirm the desorption of molecules upon heating, characterization by XRD and Fourier transform infrared spectroscopy (FT-IR; Thermo Scientific Nicolet iS50) was carried out on the $Cs_2[Mo_6Cl_{14}]$ powder both before and after heat treatment under different atmospheres. FT-IR measurements were performed with a diffuse reflectance setup, using sample powders dispersed in KBr powder.

NPD measurements were carried out to complement the XRD data because of different atomic scattering lengths. Measurements were carried out at the Institut Laue-Langevin (ILL), in Grenoble, France. A diffraction pattern of the as-prepared sample was collected at room temperature using a one-dimensional curved multidetector D1b (λ = 0.252 nm). Structural parameters of the $Cs_2[Mo_6Cl_{14}]$ lattice were analyzed by Rietveld profile refinement using the FullProf and WinPlotr software packages.[31,32] According to the literature,[33] the coherent neutron scattering lengths (b_c) adopted for the refinement were as follows: Cs, 5.42 fm; Mo, 6.715 fm; and Cl, 9.577 fm.

As the non-centrosymmetric lattice structure exhibited SHG behavior,[34]

photoluminescence studies using high excitation conditions were performed to examine if $Cs_2[Mo_6Cl_{14}]$ also exhibited SHG behavior. These studies were performed at room temperature using an optical parametric amplifier (Spectra Physics TOPAS Prime) excited by a titanium sapphire regenerative (Ti-Sap) amplifier (Spectra Physics Solstice) as the excitation light source, with 100 fs pulse width, 1 kHz repetition rate, 1.0 mJ/(pulse·cm^2) excitation density, and wavelengths of 1000 and 1200 nm. Sample luminescence was monitored using a spectrometer (Jovan-Ybon Triax550) equipped with a charge-coupled device (Andor Technology DU420A).

2.3 Computational methods

As two possible structural models have been proposed for the trigonal $Cs_2[Mo_6Cl_{14}]$ (see Fig. 1), DFT calculations were performed to compare the total energies of each model. The model shown in Fig. 1(a) represents the $P31c$ space group exhibiting lack of inversion symmetry, while that in Fig. 1(b) represents the $P\bar{3}1c$ space group, which exhibits an inversion center. Previously reported crystal structure parameters[5,28,35] were used for construction of the model with $P31c$ symmetry, while the model with $P\bar{3}1c$ symmetry was constructed according to the crystal structure of $Cs_2[Mo_6I_{14}]$, which exhibits $P\bar{3}1c$ symmetry.[29] These two models were used for the DFT structural relaxation studies.

The CASTEP code,[36] based on the plane wave pseudo-potential method,[37] was used for DFT calculations. In this study, norm-conserved pseudo-potentials (NCPPs)[38] were generated using the OPIUM code.[39] Generalized gradient approximation (GGA)[40] was selected as the exchange-correlation functional for total energy calculations. In particular, the GGA functional optimized for solid-state compounds, i.e., the PBEsol functional,[41] was used for the majority of calculations. Energy minimizations were performed using Pulay's density mixing scheme.[42] In some cases, the all-bands/EDFT method[43] was adopted to confirm the convergence of calculations using Pulay's scheme. Crystal structures were relaxed using the quasi-Newton method with the Broyden-Fletcher-Goldfarb-Shanno Hessian update scheme.[44] Polarization of electron spin was considered for all DFT calculations. The plane wave cut-off energy was set at 830 eV, while the Monkhorst-Pack grid[45,46] (4×4×3 mesh) was used for Brillouin zone sampling, and a 96×96×144 mesh was adopted for the fast Fourier transformation. The convergence tolerances were set to 5×10^{-5} nm for atomic displacement, 5×10^{-6} eV/atom for total energy, 0.1 eV/nm for maximum interatomic force, and 0.02 GPa for pressure. The effective charges of all atoms and ions were calculated using the Mulliken population method.[47,48]

Structural optimization for the models assuming $P\bar{3}1c$ and $P31c$ space groups was performed by two different means. Firstly, the fully relaxed crystal structure was obtained to determine the unstrained structure with assumed lattice symmetry. Secondly, relaxation of atomic positions with fixed lattice parameters was carried out by fixing the lattice parameters to experimentally obtained values. In addition, structural optimization without any symmetry constraints ($P1$ group) was performed to examine the possibility of symmetry lowering during the structural relaxation. On calculation of the $P1$-models, we used the models possessing $P\bar{3}1c$ or $P31c$ symmetry as initial structures, and all lattice parameters and atomic positions were relaxed to determine the fully relaxed structure. As we considered the model with $P1$ symmetry, a conventional unit cell (Z=2) was used for all calculations, although this required relatively large computational resources.

Simulation of XRD patterns using crystal structure parameters determined by DFT calculations was performed using the Mercury code (Cambridge Crystallographic Data Centre) to examine the agreement between the calculated and observed XRD patterns. In addition, following structural optimization by DFT, lattice symmetry was examined using the ADDSYM subroutine in PLATON,[49,50] which enabled us to observe symmetry elements in the relaxed structures.

3. Results and discussion

3.1 Sample characterization and purification

The obtained powder XRD patterns shown in Fig. 2 were identified by assuming that one of the two models shown in Fig. 1 was the major phase. Considering this assumption, some weak diffraction peaks could not be assigned to the trigonal $Cs_2[Mo_6Cl_{14}]$, as indicated by the arrows in Fig. 2. The intensities of these minor peaks decreased upon heating, while the relative intensities of peaks corresponding to the major phase remained relatively constant. This suggests that the unidentified XRD peaks are assignable to additional phase(s) that decomposed upon heating. The majority of the discussion will therefore focus only on the XRD peaks assigned to the trigonal $Cs_2[Mo_6Cl_{14}]$. As shown in Table I, the lattice parameters of the trigonal $Cs_2[Mo_6Cl_{14}]$ were altered by thermal treatment. The *a*-axis clearly shrank upon heat treatment, while the *c*-axis expanded, resulting in a decrease in unit cell volume upon heating. Interestingly, the lattice parameters of our as-prepared sample were close to those reported by Healy et al.,[28] while the parameters corresponding to the sample following heat treatment were comparable to those reported by Potel et al.[5] The latter phase was prepared starting from CsCl and $MoCl_2$ in a silica container using solid-state

techniques at high temperatures, thus preventing the insertion of water in the lattice. Indeed, the higher unit cell volume reported in the literature[28] and in the as-prepared sample prior to heating may be attributed to the insertion of water molecules as described below.

FT-IR measurements indicate that changes in lattice parameters correlated with the desorption of H_2O upon heating, as desorption occurred by heating under dry N_2 gas. As shown in Fig. 3, the modes at 1100–1300 cm^{-1} and 1600 cm^{-1} correspond to H_2O bending,[51] while the broad band at ~3500 cm^{-1} correlates with O-H stretching.[51] The presence of such bands indicates that the as-prepared sample contained water molecules. In some complex compounds, such as $Cs_2[Mo_6Cl_{14}]\cdot 3H_2O$, the water molecules are stabilized, forming a hydrogen bond to the Cl^- ion at the apical site (X^a).[52] Thus, the insertion of water molecules at interstitial positions could explain the relatively large unit cell volume of the as-prepared sample. In addition, a further vibrational mode found at 1700 cm^{-1} was assigned to the asymmetric bending of $(H_3O)^+$.[53] Assuming that this charged species was incorporated into the $Cs_2[Mo_6Cl_{14}]$ lattice, the substitution of $(H_3O)^+$ for a Cs^+ ion is possible. This is a reasonable consideration, as the size (0.113 nm ionic radius)[54] and positive charge of $(H_3O)^+$ are comparable with those of the Cs^+ ion (0.169 nm ionic radius).[54] Furthermore, the desorption of $(H_3O)^+$ by heat treatment could account for the changes in lattice parameters upon heating. As the lattice parameters following 1 h of treatment in pure N_2 gas were similar to those after 3 h, it appears that the rate of $H_2O/(H_3O)^+$ desorption from the lattice was rapid.

Based on these heat treatment results, we concluded that the as-prepared sample contained a number of impurities, and, hence, the sample powder heated in dry N_2 gas at 200 °C for 3 h to achieve water desorption represents the intrinsic nature of the trigonal $Cs_2[Mo_6Cl_{14}]$.

3.2 DFT calculations

The electronic structure calculations and structural optimizations were well converged for both assumed crystal structures (see Fig. 1). Indeed, the calculation initiated using the $P31c$ space group model converged to the corresponding structure even when calculations were performed in the absence of symmetrical constraints (i.e., the $P1$ space group). Furthermore, the calculation initiated from the $P\bar{3}1c$ symmetry model converged into the corresponding structure without breaking any symmetrical elements, regardless of the symmetry constraint, indicating that the results of structural relaxation strongly depend on the initial structure prior to relaxation.

The structural parameters of the fully relaxed lattice are summarized in Table II. The calculations using fixed lattice parameters were also well converged. As previously mentioned, the optimization of atomic positions with fixed lattice parameters, i.e., a_0 = 0.9789 nm and c_0 = 1.4214 nm, was considered to enable direct comparison of the structure determined by DFT optimization to the experimental results shown in Table I. The results of calculations with fixed lattice parameters are also shown in Table II. Note that the obtained structures calculated without symmetry constraints ($P1$ symmetry) were identical to those obtained with structural constraints. It should also be noted that the Mo-Mo and Mo-Cl distances in the $[Mo_6Cl_{14}]^{2-}$ complex determined by DFT structural optimization remained constants with variation in the lattice parameters, although such changes resulted in variation of the Cs-Cl distance along the *c*-axis. The interatomic distances of the optimized structure are shown in Table SI (see supplementary data). The structural parameters will be discussed in further detail below.

The calculated total energy (enthalpy) of the optimized lattice possessing $P31c$ symmetry was 6×10^{-3} eV smaller than that of the optimized lattice with $P\bar{3}1c$ symmetry, when both lattice parameters and fractional atomic positions were fully relaxed. In addition, the total energy for the $P\bar{3}1c$ symmetry model was 2×10^{-3} eV smaller than that of the $P31c$ symmetry model with fixed lattice parameters. These differences in total energy between the two models were very small. As the optimized lattice parameters for the two models differed, the unit cell volume (V_0) of the optimized $P\bar{3}1c$ structure was slightly smaller than that of the $P31c$ structure. This could therefore account for the lower total energy of the fully relaxed (unstressed) $P31c$ model. When considering the total energy using fixed lattice models, the slightly lower total energy of the $P\bar{3}1c$ symmetry possibly leads to a more stable structure compared to $P31c$ symmetry. This occurs as $P31c$ symmetry requires a higher compressive stress to maintain the observed lattice volume. However, such small energetic differences between the different symmetries are insufficient for determination of the $Cs_2[Mo_6Cl_{14}]$ lattice space group from the comparison of total energies alone.

Figure 4(a) shows that the total electron density of states (DOS) in the fully relaxed trigonal $Cs_2[Mo_6Cl_{14}]$ lattice possesses $P\bar{3}1c$ symmetry. Results of DOS calculations for both the lattice with $P31c$ symmetry and the model with fixed lattice parameters were comparable to those shown in Fig. 4(a). These results are consistent with previous results showing that the total energies of the two structural models were comparable. In addition, the DOS values for up-spin electrons were identical to those for down-spin electrons, and so the calculated results indicate that no magnetic behavior should be expected from the

trigonal $Cs_2[Mo_6Cl_{14}]$.

As the electronic states are highly localized, the band dispersion of electronic orbitals (*E-k* dispersion) was flat, as shown in Fig. 4(b). It was therefore not possible to determine if the band gap was direct or indirect, as the exact *k*-vector at the valence band maximum (VBM) and the conduction band maximum (CBM) could not be determined. The energy band gap deduced from the *E-k* plot was 2.46–2.48 eV, which is slightly smaller than the experimentally determined optical band gap.[12] As GGA-based DFT calculations give relatively small band gap values due to the self-interaction of electrons,[55,56] a small band gap is possible when employing conventional DFT codes.

Figure 5 shows the projected-DOS (PDOS) of $Cs_2[Mo_6Cl_{14}]$ exhibiting $P\bar{3}1c$ symmetry, which is comparable to the calculated PDOS for the *P*31*c* $Cs_2[Mo_6Cl_{14}]$. As shown in Fig. 5, the VBM consists of Mo 4*d* orbitals, and exhibits a rather wide energy dispersion in the valence band. In contrast, the Cl 3*p* orbitals are separated into two groups, with Cl^a being distributed in the top-to-middle range of the valence band, and Cl^i being located in the middle-to-bottom range. Furthermore, the electronic state of the Cs valence electrons was observed at 1–2 eV from the VBM.

The effective charge of each ion calculated by Mulliken analysis is shown in Table III. Variations in lattice symmetry and lattice parameters caused no significant changes in the effective charge of each ion. Hence, the following descriptions are common for all structural models considered in this study. The most notable result is that the effective charges at the Cl^a and Cl^i sites differ from one another. The effective charge at the Cl^a sites was more negative than that at the Cl^i sites, indicating that the Cl^a sites exhibit a greater ionic tendency. In addition, the previously mentioned differences in PDOS between the two sites along with the differences in effective charge are consistent with experimental observations. Indeed, core-level photoemission spectra of the X-anions in $A_m[Mo_6X^i_8X^a_6]$ complexes contained two peaks with an intensity ratio of approximately 3:4,[57,58] indicating that the chemical state of the six X^a ions differed from that of the eight X^i ions. Hence, the calculated electronic structure and experimental observations are in good agreement. Furthermore, from the charge analysis, the effective charge of the Cs ions was comparable to its formal charge. This suggests that the $[Mo_6Cl_{14}]^{2-}$ electronic state is highly localized, and the bonds between the complex and the Cs ions are purely ionic.

3.3 Crystallographic comparison between optimized crystal structures

Analysis using the ADDSYM subroutine suggested that the space group of the optimized

crystal lattice after full relaxation differed from that of the lattice optimized using fixed lattice parameters. The fully relaxed lattice [Table II(a), left columns] belongs to the $P31c$ space group, while the structure optimized using fixed lattice parameters [Table II(a), right columns] belongs to the $P\bar{3}1c$ space group. Both calculations were performed by applying constraints without inversion symmetry, allowing $Cs_2[Mo_6Cl_{14}]$ to maintain its non-centrosymmetry upon increasing the unit cell volume. In contrast, rearrangement of the atoms from a non-centrosymmetric to a centrosymmetric space group occurred when the lattice parameters were fixed to the experimental values. Indeed, XRD simulations employing the structural parameters optimized using the lattice with fixed $P31c$ symmetry produced similar patterns to those obtained using the lattice with fixed $P\bar{3}1c$ symmetry, and to the observed pattern for the sample following heat treatment in dry N_2 (Fig. S1 in the online supplementary data). As the removal of H_2O (H_3O^+) and/or -OH was demonstrated from FT-IR measurements, we expected that following heat treatment, the samples would be free from solvent insertion. Therefore, it is likely that the observed XRD intensity profile is closer to the intrinsic form of $Cs_2[Mo_6Cl_{14}]$, while the structural parameters calculated by DFT better represent the real $Cs_2[Mo_6Cl_{14}]$ lattice. As suggested from ADDSYM calculations and comparison of the simulated XRD patterns, the structural parameters calculated using both $P31c$ and $P\bar{3}1c$ symmetry were comparable, and so the former was considered to be the centrosymmetric structure. Therefore, the DFT calculations suggest that $P\bar{3}1c$ symmetry is the most suitable space group for the $Cs_2[Mo_6Cl_{14}]$ lattice.

3.4 High harmonic generation in luminescence

Figure 6 shows the luminescence spectra of the prepared $Cs_2[Mo_6Cl_{14}]$ upon excitation with a UV pulsed laser source ($\lambda = 410$ nm) and with an infrared (IR) pulsed laser ($\lambda = 1000$ and 1200 nm) with high power density. Furthermore, the spectrum obtained from the excitation of quartz (α-SiO_2) with an IR laser beam ($\lambda = 1000$ nm) is given as a reference. A broad emission in the visible-red region centered at $\lambda = 700$ nm was observed in all $Cs_2[Mo_6Cl_{14}]$ luminescence spectra, which can be attributed to a spontaneous luminescence peak.[10,12] This emission was also observed upon excitation using a pulsed IR beam with high excitation density. We expect that this red luminescence resulted from multi-photon absorption.

An additional emission corresponding to third harmonic generation (THG) was also observed in the spectrum obtained from excitation with IR beams (Fig. 6). However, signals corresponding to the SHG were not observed in the $Cs_2[Mo_6Cl_{14}]$ spectra despite the

excitation intensity being sufficient to excite strong SHG emission from α-SiO_2. This indicates that the Cs complex prepared herein does exhibit inversion symmetry. Considering these observations together with the DFT calculation results mentioned above, we concluded that the crystal symmetry of $Cs_2[Mo_6Cl_{14}]$ is most likely be the centrosymmetric $P\bar{3}1c$ space group.

3.5 Refinement of structural parameters with NPD

Assuming that $Cs_2[Mo_6Cl_{14}]$ belongs to the $P\bar{3}1c$ space group, the Rietveld refinement for the NPD profile was performed (the observed and peak-fitting profiles are shown in Fig. S2, supplementary data). The refinement was well-converged and the resulting reliability factors (*R*-factors) were R_{wp} = 2.19%, R_e = 0.22%, R_b = 2.70%, R_f = 2.30%, and χ^2 = 103, suggesting that the assumption of $P\bar{3}1c$ symmetry was consistent with the observed NPD pattern. The structural parameters refined from the combined NPD and XRD profiles are also shown in Table IV, indicating a consistent atomic arrangement to that determined by DFT calculations, as summarized in Table II. Hence, we concluded that the refined structural parameters accurately represent the intrinsic crystal structure of the $Cs_2[Mo_6Cl_{14}]$ complex.

4. Conclusions

Use of a range of analytical techniques revealed that the lattice parameters of $Cs_2[Mo_6Cl_{14}]$ changed upon the adsorption/desorption of water-related fragments and, hence, the sample-to-sample deference in the reported lattice parameters could be attributed to residual impurities, such as H_2O, OH^-, and H_3O^+. Desorption of these impurities was therefore carried out prior to further investigations. XRD and NPD studies showed consistent atomic arrangement to that determined from the electron density in the lattice. These crystal structures, with theoretically optimized atomic coordinates, were comparable despite imposing the centrosymmetric or non-centrosymmetric constraints. Moreover, the optical measurements monitoring high harmonic generation indicated the presence of inversion symmetry in the $Cs_2[Mo_6Cl_{14}]$ lattice. Hence, we could conclude that the structural model with $P\bar{3}1c$ symmetry was better suited to the obtained results than that with $P31c$ symmetry.

Upon comparison of crystalline phase stability based on the DFT studies, the total energy of the $Cs_2[Mo_6Cl_{14}]$ lattice with $P\bar{3}1c$ symmetry was calculated to be slightly higher than that with $P31c$ symmetry following structural relaxation. However, the lattice parameters

deduced for the model with $P31c$ symmetry were not consistent with the observed values. Furthermore, the results of total energy calculations with the model containing fixed lattice parameters indicated that the model with $P\bar{3}1c$ symmetry was more stable, due to an increase in internal energy through compressive stress. As the difference in total energy between the two symmetry models was small (i.e., several meV), it is possible that a meta-stable polymorph of the $Cs_2[Mo_6Cl_{14}]$ lattice can exist. However, considering the obtained experimental results, we concluded that the total energy calculated using the fixed lattice parameter conditions represents the actual $Cs_2[Mo_6Cl_{14}]$ cluster compound, while the $Cs_2[Mo_6Cl_{14}]$ crystallized with $P\bar{3}1c$ symmetry is the stable phase under ambient pressure.

Furthermore, impurity analysis for such metal-cluster-complex compounds must be carefully performed to determine the real nature of these compounds. Indeed, the lattice parameters exhibited significant changes upon the desorption of water-related molecules. Consideration of the desorption behavior is therefore important not only for scientific investigations but also in terms of engineering applications. For instance, for LED phosphor applications, thermal stability is necessary to achieve high power operations.

Finally, as DFT has been shown to effectively reproduce the stable atomic arrangement of the metal cluster compounds, we plan to focus on the understanding and control of the luminescence properties of the compounds reported herein.

Acknowledgments

The authors thank those involved in UMI-LINK and its related activities, particularly Dr. Mari Kono and Dr. Benjamin Dierre, of Saint-Gobain KK (Tokyo, Japan), and N. Dumait, Serge Paofai, and Dr. T. Roisnel of ISCR for their contributions to the management of UMI-LINK. N.S. would also like to thank Professor Junzo Tanaka of Tokyo Tech. for support and encouragement. P.L. and S.C. are indebted to the Institut Laue-Langevin (Grenoble, France) for the provision of research facilities. Parts of this study have been financially supported by ANR (CLUSTOP-11-BS08-013-01) and Fondation Langlois.

References

1) A. Perrin, C. Perrin, and M. Sergent, J. Less Common Met. **137**, 241 (1988).
2) W. Preetz, K. Harder, H. G. V. Schnering, G. Kliche, and K. Peters, J. Alloys Compd. **183**, 413 (1992).
3) W. Preetz, D. Bublitz, H. G. V. Schnering, and J. Saßmannshausen, Z. Anorg. Allg. Chem. **620**, 234 (1994).
4) P. Brückner, W. Preetz, and M. Pünjer, Z. Anorg. Allg. Chem. **623**, 8 (1997).
5) M. Potel, C. Perrin, A. Perrin, and M. Sergent, Mater. Res. Bull. **21**, 1239 (1986).
6) G. Saito, H. Hosoda, Y. Yoshida, J. Hagiwara, K. Nishimura, H. Yamochi, A. Otsuka, T. Hiramatsu, Y. Shimazaki, K. Kirakci, S. Cordier, and C. Perrin, J. Mater. Chem. **22**, 19774 (2012).
7) S. Cordier, F. Grasset, Y. Molard, M. Amela-Cortes, R. Boukherroub, S. Ravaine, M. Mortier, N. Ohashi, N. Saito, and H. Haneda, J. Inorg. Organomet. Polym. Mater. **25**, 189 (2015).
8) R. Chevrel, M. Hirrien, and M. Sergent, Polyhedron **5**, 87 (1986).
9) O. Fischer, A. Treyvaud, R. Chevrel, and M. Sergent, Solid State Commun. **17**, 721 (1975).
10) A. W. Maverick, and H. B. Gray, J. Am. Chem. Soc. **103**, 1298 (1981).
11) T. Aubert, N. Nerambourg, N. Saito, H. Haneda, N. Ohashi, M. Mortier, S. Cordier, and F. Grasset, Part. Part. Syst. Charact. **30**, 90 (2013).
12) F. Grasset, F. Dorson, S. Cordier, Y. Molard, C. Perrin, A.-M. Marie, T. Sasaki, H. Haneda, Y. Bando, and M. Mortier, Adv. Mater. **20**, 143 (2008).
13) A. Barras, S. Cordier, and R. Boukherroub, Appl. Catal. B **123-124**, 1 (2012).
14) A. Barras, M. R. Das, R. R. Devarapalli, M. V. Shelke, S. Cordier, S. Szunerits, and R. Boukherroub, Appl. Catal. B **130-131**, 270 (2013).
15) P. Kumar, S. Kumar, S. Cordier, S. Paofai, R. Boukherroub, and S. L. Jain, RSC Adv. **4**, 10420 (2014).
16) R. N. Ghosh, P. A. Askeland, S. Kramer, and R. Loloee, Appl. Phys. Lett. **98**, 221103 (2011).
17) S. Ye, F. Xiao, Y. X. Pan, Y. Y. Ma, and Q. Y. Zhang, Mater. Sci. Eng. R **71**, 1 (2010).
18) R.-J. Xie, N. Hirosaki, N. Kimura, K. Sakuma, and M. Mitomo, Appl. Phys. Lett. **90**, 191101 (2007).
19) K. Costuas, A. Garreau, A. Bulou, B. Fontaine, J. Cuny, R. Gautier, M. Mortier, Y. Molard, J.-L. Duvail, E. Faulques, and S. Cordier, Phys. Chem. Chem. Phys. **17**, 28574 (2015).
20) T. C. Zietlow, M. D. Hopkins, and H. B. Gray, J. Solid State Chem. **57**, 112 (1985).

21) J. A. Jackson, C. Turro, M. D. Newsham, and D. G. Nocera, J. Phys. Chem. **94**, 4500 (1990).
22) L. M. Robinson, R. L. Bain, D. F. Shriver, and D. E. Ellis, Inorg. Chem. **34**, 5588 (1995).
23) R. Ramirez-Tagle, and R. Arratia-Pérez, Chem. Phys. Lett. **460**, 438 (2008).
24) R. Ramirez-Tagle, and R. Arratia-Pérez, Chem. Phys. Lett. **455**, 38 (2008).
25) T. G. Gray, Chem. Eur. J. **15**, 2581 (2009).
26) J. S. Gancheff, and P. A. Denis, J. Phys. Chem. A **115**, 211 (2011).
27) T. G. Gray, C. M. Rudzinski, E. E. Meyer, and D. G. Nocera, J. Phys. Chem. A **108**, 3238 (2004).
28) P. C. Healy, D. L. Kepert, D. Taylor, and A. H. White, J. Chem. Soc., Dalton Trans. **6**, 646 (1973).
29) K. Kirakci, S. Cordier, and C. Perrin, Z. Anorg. Allg. Chem. **631**, 411 (2005).
30) F. W. Koknat, T. J. Adaway, S. I. Erzerum, and S. Syed, Inorg. Nucl. Chem. Lett. **16**, 307 (1980).
31) J. Rodríguez-Carvajal, Physica B **192**, 55 (1993).
32) T. Roisnel, and J. Rodríguez-Carvajal, Mater. Sci. Forum **378–381**, 118 (2001).
33) V. F. Sears, Neutron News **3**, 26 (1992).
34) S. K. Kurtz, and T. T. Perry, J. Appl. Phys. **39**, 3798 (1968).
35) Pearson's Crystal Data, ASM International, Ohio, 2014, No. 1928748.
36) S. J. Clark, M. D. Segall, C. J. Pickard, P. J. Hasnip, M. I. J. Probert, K. Refson, and M. C. Payne, Z. Kristallogr. **220**, 567 (2005).
37) V. Milman, B. Winkler, J. A. White, C. J. Pickard, M. C. Payne, E. V. Akhmatskaya, and R. H. Nobes, Int. J. Quantum Chem. **77**, 895 (2000).
38) D. R. Hamann, M. Schlüter, and C. Chiang, Phys. Rev. Lett. **43**, 1494 (1979).
39) A. W. Rappe, K. M. Rabe, E. Kaxiras, and J. D. Joannopoulos, Phys. Rev. B **41**, 1227 (1990).
40) J. P. Perdew, K. Burke, and M. Ernzerhof, Phys. Rev. Lett. **77**, 3865 (1996).
41) J. P. Perdew, A. Ruzsinszky, G. I. Csonka, O. A. Vydrov, G. E. Scuseria, L. A. Constantin, X. Zhou, and K. Burke, Phys. Rev. Lett. **100**, 136406 (2008).
42) P. Pulay, Chem. Phys. Lett. **73**, 393 (1980).
43) M. C. Payne, M. P. Teter, D. C. Allan, T. A. Arias, and J. D. Joannopoulos, Rev. Mod. Phys. **64**, 1045 (1992).
44) B. G. Pfrommer, M. Côté, S. G. Louie, and M. L. Cohen, J. Comput. Phys. **131**, 233 (1997).

45) H. J. Monkhorst, and J. D. Pack, Phys. Rev. B **13**, 5188 (1976).
46) J. D. Pack, and H. J. Monkhorst, Phys. Rev. B **16**, 1748 (1977).
47) M. D. Segall, R. Shah, C. J. Pickard, and M. C. Payne, Phys. Rev. B **54**, 16317 (1996).
48) M. D. Segall, P. J. D. Lindan, M. J. Probert, C. J. Pickard, P. J. Hasnip, S. J. Clark, and M. C. Payne, J. Phys.: Condens. Matter **14**, 2717 (2002).
49) Y. L. Page, J. Appl. Crystallogr. **20**, 264 (1987).
50) Y. L. Page, J. Appl. Crystallogr. **21**, 983 (1988).
51) J. R. Ferraro, and A. Walker, J. Chem. Phys. **42**, 1278 (1965).
52) A. Flemström, T. K. Hirsch, L. Eriksson, and S. Lidin, Solid State Sci. **6**, 509 (2004).
53) M. Falk, and P. A. Giguère, Can. J. Chem. **35**, 1195 (1957).
54) Y. Marcus, J. Solution Chem. **12**, 271 (1983).
55) J. P. Perdew, and A. Zunger, Phys. Rev. B **23**, 5048 (1981).
56) J. Heyd, J. E. Peralta, G. E. Scuseria, and R. L. Martin, J. Chem. Phys. **123**, 174101 (2005).
57) R. A. Walton, J. Less-Common Met. **54**, 71 (1977).
58) S. A. Best, and R. A. Walton, Inorg. Chem. **18**, 484 (1979).

Figure Captions

Fig. 1. (Color online) Trigonal $Cs_2[Mo_6Cl_{14}]$ unit cell. (a) $P31c$ space group, and (b) $P\bar{3}1c$ space group.

Fig. 2. (Color online) Powder XRD patterns of $Cs_2[Mo_6Cl_{14}]$ before and after thermal treatment in air and under dry N_2. Arrows denote diffraction peaks originating from the secondary phase.

Fig. 3. (Color online) FT-IR spectra of $Cs_2[Mo_6Cl_{14}]$ powders both before and after thermal treatment in air and under dry N_2.

Fig. 4. (Color online) (a) Density of states and (b) band dispersion in $Cs_2[Mo_6Cl_{14}]$ with $P\bar{3}1c$ symmetry.

Fig. 5. (Color online) Projected density of state of $Cs_2[Mo_6Cl_{14}]$ crystallized in $P\bar{3}1c$ symmetry.

Fig. 6. (Color online) Luminescence spectra of $Cs_2[Mo_6Cl_{14}]$ under strong excitation with an IR laser beam (λ = 1000 and 1200 nm) and under weaker excitation with a UV laser beam (λ = 410 nm). The spectrum of α-SiO_2 under IR laser irradiation (λ = 1000 nm) is given as a reference.

Table I. Refined lattice parameters for $Cs_2[Mo_6Cl_{14}]$ both before and after thermal treatment.

Annealing conditions			Lattice parameters		
Temperature (°C)	Atmosphere	Period (h)	a_0 / nm	c_0 / nm	V_0 / nm^3
N/A (As prepared)			0.9833(1)	1.4185(3)	1.1878(2)
150	air	1.0	0.9803(1)	1.4193(3)	1.1811(2)
200	dry-N_2	1.0	0.9789(1)	1.4210(1)	1.1793(2)
200	dry-N_2	3.0	0.9789(1)	1.4214(2)	1.1796(2)
References					
Potel et al.[5)]			0.977	1.422	1.176
Healy et al.[28)]			0.983(5)	1.431(3)	1.198

Table II. Summary of the theoretically optimized $Cs_2[Mo_6Cl_{14}]$ structure: (a) $P31c$ symmetry and (b) $P\bar{3}1c$ symmetry crystal structure following structural optimization by DFT calculations.

(a)

Lattice constants	Fully relaxed			Fixed lattice parameters		
a_0 / nm	0.980			0.979		
c_0 / nm	1.499			1.421		
V_0 / nm^3	1.246			1.180		
Fractional atomic positions						
Atom	Wyck.	x	y	z	x	y	z
Mo1	6*c*	0.509	0.180	0.214	0.510	0.178	0.210
Mo2	6*c*	0.515	0.340	0.357	0.513	0.337	0.361
Cl1	6*c*	0.031	0.332	0.126	0.039	0.342	0.120
Cl2	6*c*	0.312	0.355	0.444	0.308	0.351	0.451
Cl3	6*c*	0.368	0.048	0.354	0.371	0.045	0.358
Cl4	6*c*	0.379	0.342	0.217	0.375	0.334	0.213
Cl5	2*b*	0.333	0.667	0.987	0.333	0.667	0.997
Cl6	2*b*	0.333	0.667	0.584	0.333	0.667	0.574
Cs1	2*b*	0.333	0.667	0.313	0.333	0.667	0.294
Cs2	2*a*	0	0	0.029	0	0	0.031

(b)

Lattice constants		Fully relaxed			Fixed lattice parameters		
a_0 / nm		0.980			0.979		
c_0 / nm		1.475			1.421		
V_0 / nm^3		1.227			1.180		
Fractional atomic positions							
Atom	Wyck.	*x*	*y*	*z*	*x*	*y*	*z*
Mo1	12*i*	0.666	0.177	0.177	0.666	0.177	0.175
Cl1	4*f*	0.667	0.333	0.046	0.667	0.333	0.038
Cl2	12*i*	0.957	0.330	0.180	0.957	0.330	0.177
Cl3	12*i*	0.654	–0.039	0.090	0.653	–0.042	0.085
Cs1	2*c*	0.667	0.333	0.75	0.667	0.333	0.75
Cs2	2*b*	0	0	0	0	0	0

Table III. List of Mulliken populations in the calculated structure of $Cs_2[Mo_6Cl_{14}]$: atomic populations in (a) $P31c$ symmetry and (b) $P\bar{3}1c$ symmetry.

(a)

Atom	*s*	*p*	*d*	Total	Charge (*e*)
Mo1	2.41	6.37	5.01	13.79	0.21
Mo2	2.41	6.39	5.01	13.81	0.19
Cl1	1.94	5.46	0	7.40	–0.40
Cl2	1.93	5.47	0	7.40	–0.40
Cl3	1.93	5.17	0	7.10	–0.10
Cl4	1.93	5.16	0	7.09	–0.09
Cl5	1.94	5.12	0	7.06	–0.06
Cl6	1.93	5.13	0	7.06	–0.06
Cs1	2.05	5.94	0	7.99	1.01
Cs2	2.08	5.99	0	8.07	0.93

(b)

Atom	*s*	*p*	*d*	Total	Charge (*e*)
Mo1	2.41	6.38	5.01	13.80	0.20
Cl1	1.93	5.12	0	7.05	–0.05
Cl2	1.93	5.17	0	7.10	–0.10
Cl3	1.94	5.46	0	7.40	–0.40
Cs1	2.05	5.95	0	8.00	1.00
Cs2	2.08	5.99	0	8.07	0.93

Table IV. Crystallographic parameters of the trigonal $Cs_2[Mo_6Cl_{14}]$ with $P\bar{3}1c$ symmetry refined by combined neutron and X-ray powder diffraction.

Lattice constants						
a_0 / nm	0.9805(1)					
c_0 / nm	1.4170(2)					
V_0 / nm^3	1.1796(2)					
Fractional atomic positions						
Atom	Wyck.	x	y	z	Occ.	U_{iso}
Mo1	12*i*	0.663(1)	0.177(1)	0.175(1)	1.0	0.0190(3)
Cl1	4*f*	2/3	1/3	0.039(1)	1.0	0.0203(3)
Cl2	12*i*	0.956(1)	0.330(1)	0.178(1)	1.0	0.0190(3)
Cl3	12*i*	0.655(1)	–0.035(1)	0.085(1)	1.0	0.0368(3)
Cs1	2*c*	2/3	1/3	0.75	1.0	0.0317(5)
Cs2	4*e*	0	0	0.028(2)	0.5	0.0317(5)

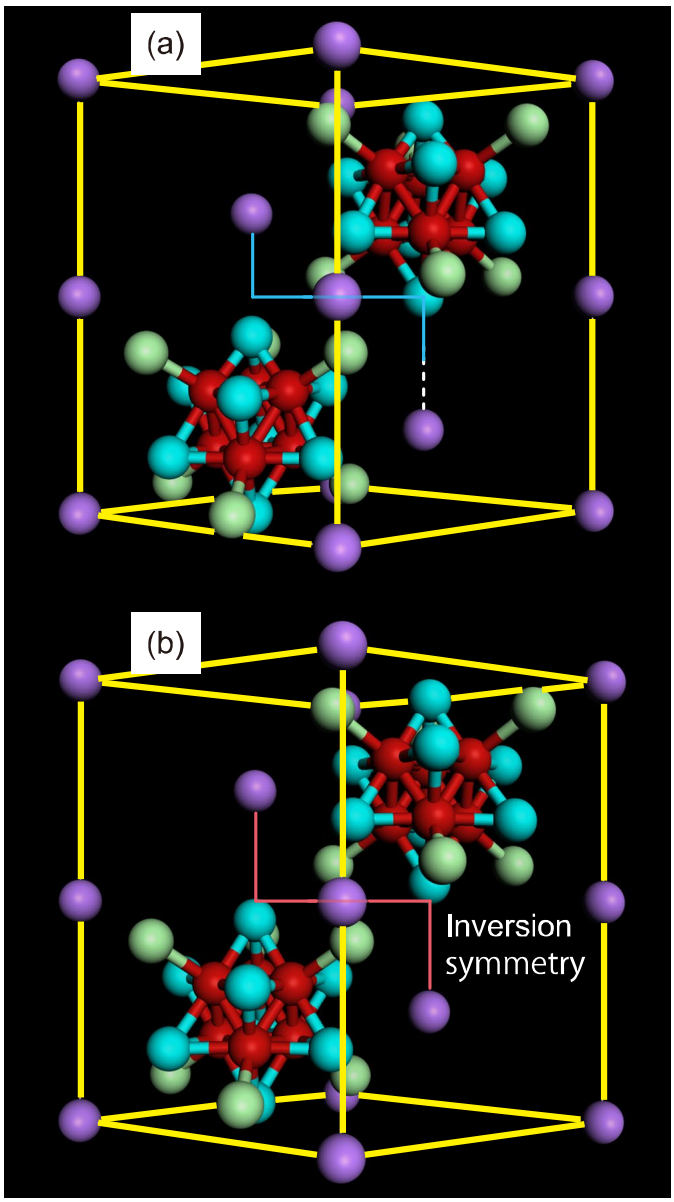

Fig. 1. (Color online) Trigonal $Cs_2[Mo_6Cl_{14}]$ unit cell. (a) $P31c$ space group, and (b) $P\bar{3}1c$ space group.

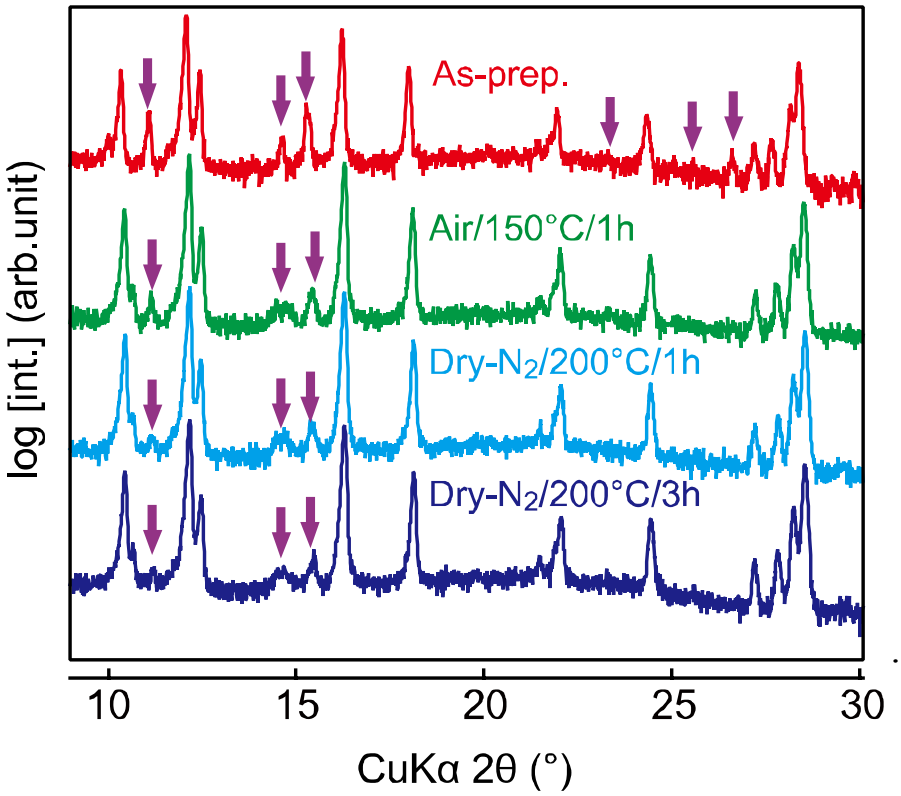

Fig. 2. (Color online) Powder XRD patterns of $Cs_2[Mo_6Cl_{14}]$ before and after thermal treatment in air and under dry N_2. Arrows denote diffraction peaks originating from the secondary phase.

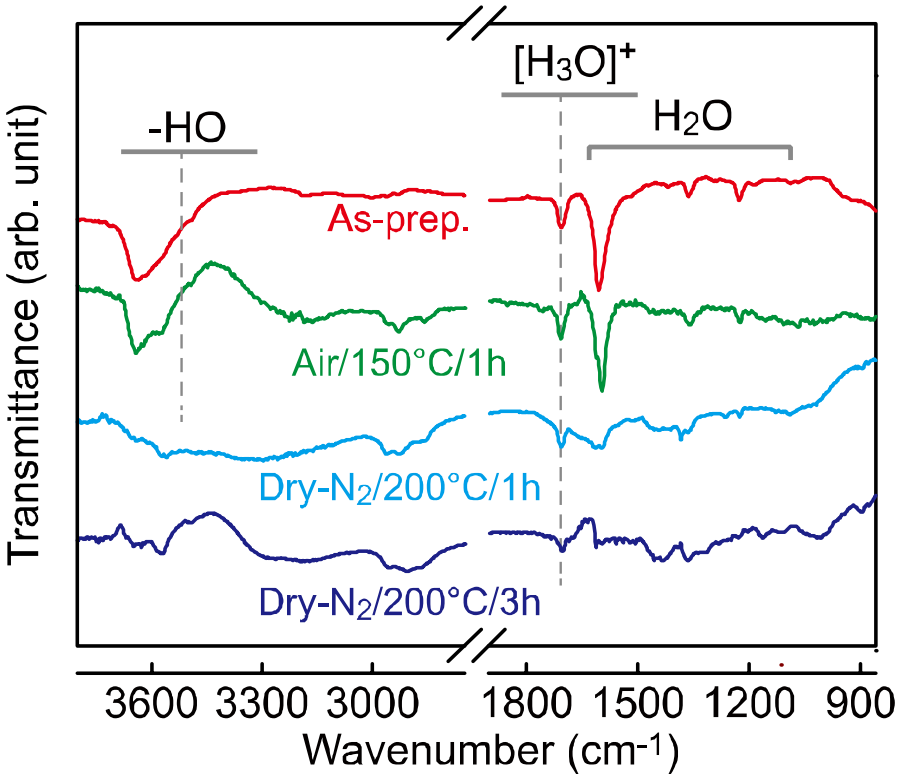

Fig. 3. (Color online) FT-IR spectra of $Cs_2[Mo_6Cl_{14}]$ powders both before and after thermal treatment in air and under dry N_2.

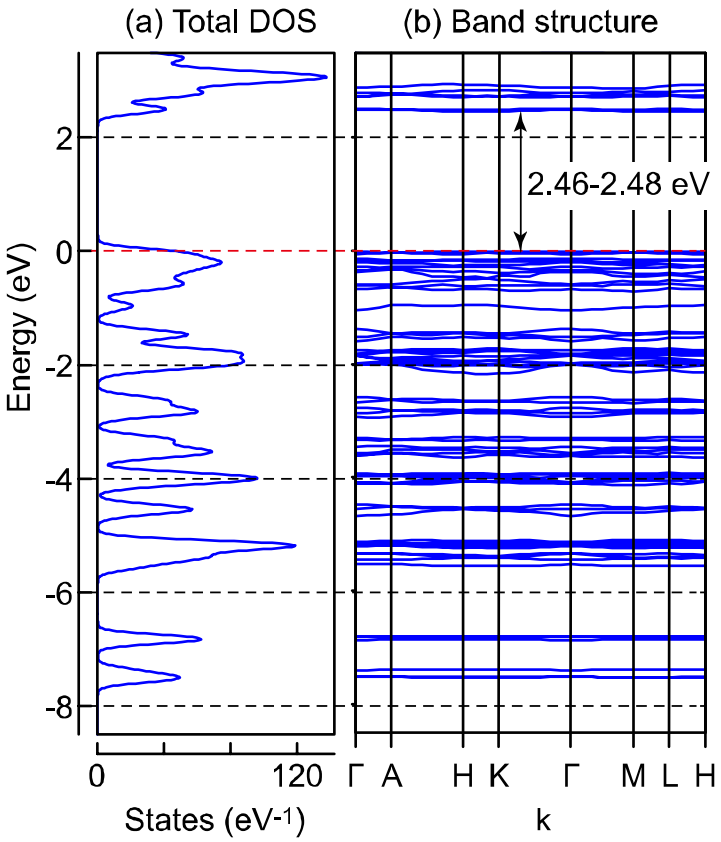

Fig. 4. (Color online) (a) Density of states and (b) band dispersion in $Cs_2[Mo_6Cl_{14}]$ with $P\bar{3}1c$ symmetry.

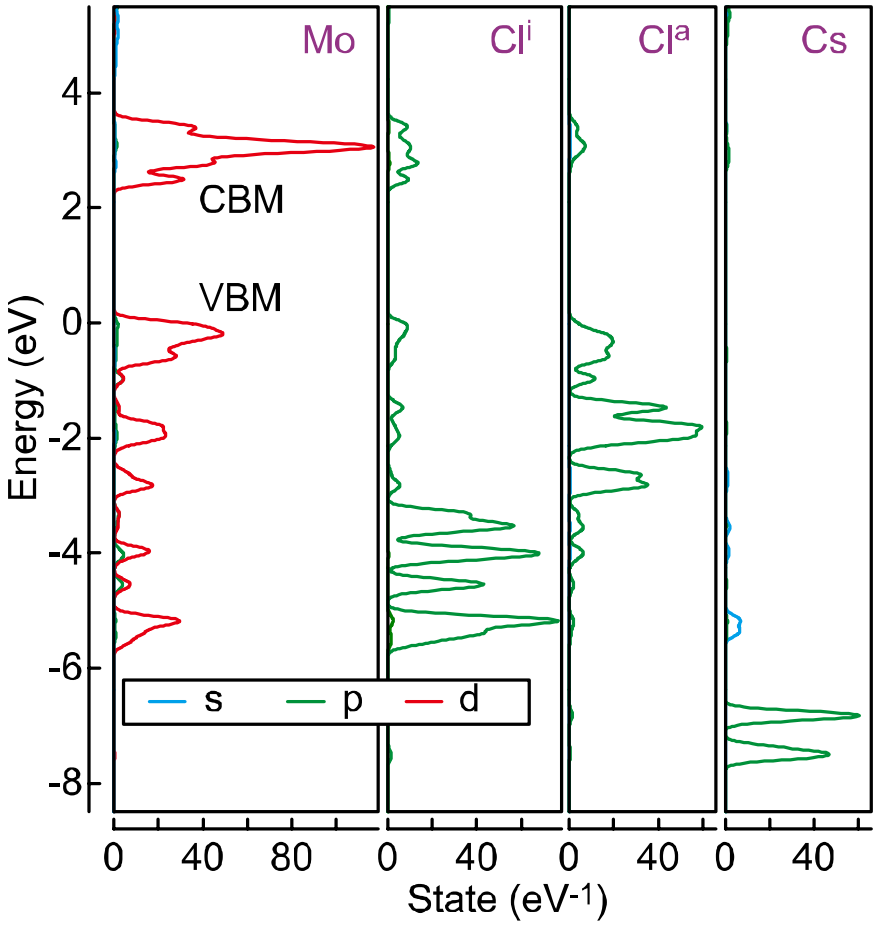

Fig. 5. (Color online) Projected density of state of $Cs_2[Mo_6Cl_{14}]$ crystallized in $P\bar{3}1c$ symmetry.

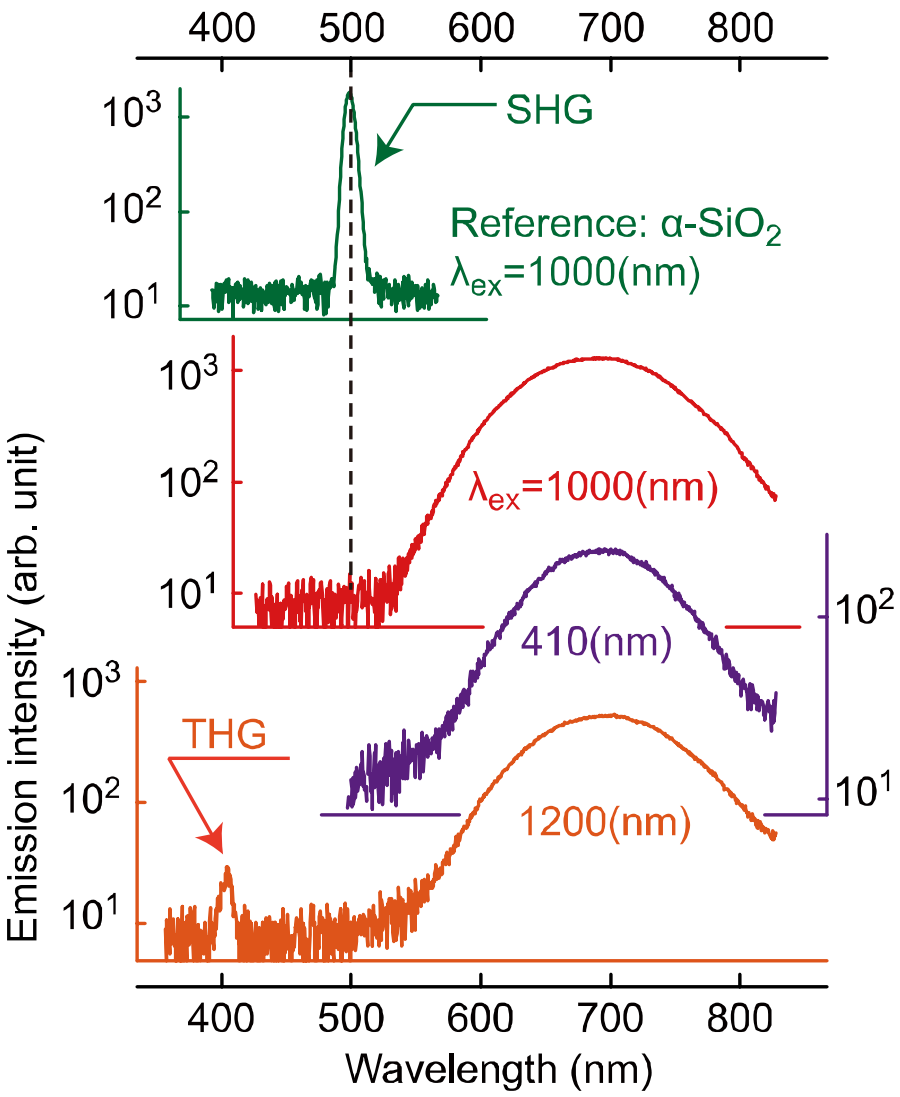

Fig. 6. (Color online) Luminescence spectra of $Cs_2[Mo_6Cl_{14}]$ under strong excitation with an IR laser beam (λ = 1000 and 1200 nm) and under weaker excitation with a UV laser beam (λ = 410 nm). The spectrum of α-SiO_2 under IR laser irradiation (λ = 1000 nm) is given as a reference.